Materials Science & Engineering A 707 (2017) 602–611

Contents lists available at ScienceDirect

Materials Science & Engineering A

journal homepage: www.elsevier.com/locate/msea

Strong ductile bulk tungsten

Z.S. Levin[a,b,*], K.T. Hartwig[a]

[a] Texas A & M University, College Station, TX, USA
[b] Air Force Research Lab, Space Vehicles Directorate Kirtland, New Mexico, USA

ARTICLE INFO

Keywords:
Tungsten
Ductility
Strength
Equal channel angular extrusion
Sever plastic deformation
Mechanical properties

ABSTRACT

Tungsten has long faced the problem of limited to no ductility in bulk polycrystalline form, due in part to the low energy needed for intergranular fracture. This limited ductility can be overcome through processing by dramatically reducing the cross sectional area following a conventional temperature step-down method that improves ductility through elongation of grain boundaries and development of a {110} fiber texture along the length of the material. While this technology is over 100 years old, little progress has been made to improve the ductility of bulk material. In the current investigation plastically deformed bulk tungsten was observed to have a room temperature tensile ductility between 17% and 23% total elongation at failure in bend specimens, and a flexural yield strength near ~ 3 GPa. This improvement in ductility following multipass equal channel angular extrusion processing appears to be caused by a similarity in microstructure and texture to that of ductile tungsten wire. The onset temperature for transition to noticeable ductility is seen to decrease dramatically with the level of plastic strain. The results indicate that severe plastic deformation processing at low homologous temperatures may be an effective way to improve the ductility and toughness of bulk tungsten and other brittle crystalline metals.

1. Introduction

The refractory transition metal tungsten (W) is known primarily for its high density (19.25 g/cc) and high melting point (3422 °C). Tungsten also has a high compressive strength, a high Young's modulus (411 MPa), and a high tensile yield stress (3920 MPa) when drawn to wire [1]. The largest present-day application for tungsten is in the fabrication of tungsten-carbide, a hard material used in cermet cutting tools, for hard-surface components, and for strengthening in iron and nickel based alloys. The special properties of tungsten make it attractive for many applications including cobalt cermet for cutting tools, ballistic projectiles, radiation shielding, ballast weights, and most recently for diffusion barriers in integrated circuits [2]. Despite attractive physical properties, tungsten has found limited use for structural applications because of poor ductility.

Tungsten has the body centered cubic crystal structure, and a ductile-to-brittle transition temperature (DBTT) between 200 and 300 °C [1]. This transition temperature is influenced by working [3–6], orientation [7], texture [8–10], strain rate [11], heat treatment [12], impurities [13,14], test mode [15], and stress concentration [16,17].

In bulk tungsten, poor ductility stems from two characteristics: a preference for intergranular separation caused by weak or embrittled grain boundaries, and a limited number of active slip systems below the ductile-to-brittle transition temperature (DBTT) [18]. In annealed polycrystalline tungsten, failure is dominated by this low energy intergranular separation, because this mode of failure requires less energy than the cleavage of the tungsten crystal lattice (referred to as transgranular cleavage). Elongation of the original grain boundaries through warm working can mitigate this low energy failure mode, where grains have sufficient length to interrupt intergranular crack propagation [19]. Processing to impart such a microstructure is typically done though swaging [3], rolling [14,20–23], and area reduction extrusion at temperatures near but not exceeding the recrystallization temperature [24]. However, while possessing higher fracture toughness at elevated temperatures, tungsten often remains brittle at ambient temperatures and can have a higher DBTT than the unworked material [8]. This behavior is in part attributed to the generation of numerous dislocations during working, which act as barriers for mobile dislocations.

The limited number of active slip systems is the other primary cause of poor ductility in polycrystalline tungsten. In single crystal experiments it was shown that tungsten possess two primary crack propagation systems: along the {100} and {110} planes. It was shown that the {100} planes possess roughly half the fracture toughness of the {110} planes [18]. The higher fracture toughness of the {110} crack system is attributed to the greater nucleation and propagation of dislocations away from the high stress field near a crack tip on the {110} planes,

* Corresponding author.
E-mail address: zlevin1@tamu.edu (Z.S. Levin).

http://dx.doi.org/10.1016/j.msea.2017.09.100
Received 27 June 2017; Received in revised form 20 September 2017; Accepted 21 September 2017
Available online 22 September 2017

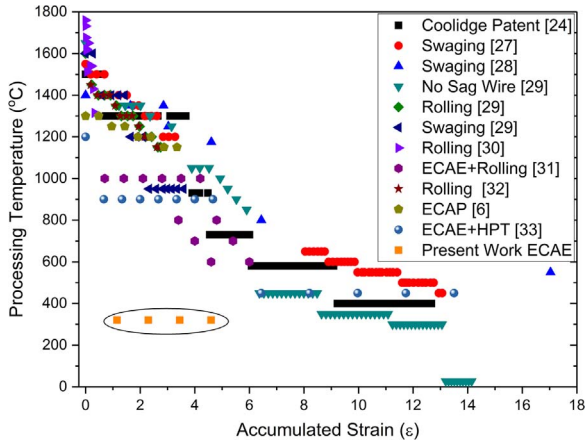

Fig. 1. Tungsten processing data from the literature and this work, converted to accumulated strain at each processing temperature. References [6,24,28–34].

producing blunting of the crack tip. It is only when tungsten has been sufficiently worked that this favorable [110] texture is generated. In order to produce this effect with traditional processing techniques involving oriented deformation, the cross section of bulk material must be reduced substantially, a circumstance that may be undesirable.

William D. Coolidge developed a technique for improving the ductility of tungsten wire for incandescent light bulb filaments and described the process in his 1913 patent on ductile tungsten [24]. This tungsten wire with increased toughness and ductility over previous filament materials was produced through a temperature step down approach illustrated in Fig. 1. For this figure, area reduction is converted into accumulated strain at each processing temperature to allow for comparisons between processing methods for different tungsten products. Various results are shown in Fig. 1 along with the Coolidge patent temperature reduction sequence. The original Coolidge approach involved compacting reduced tungsten powder, followed by sintering through self-resistance heating in a hydrogen atmosphere. The sintered rod was then swaged, area-reduction extruded, and finally drawn at progressively lower temperatures until a wire capable of being spooled and bent was produced. It would only be later in the work by Zay Jeffries [25], that the improved ductility was understood and attributed to the development of an elongated fibrous microstructure. Further work showed that the [110] fiber texture was the main reason for improved ductility [22,26,27].

More recent efforts to improve the strength and ductility of bulk tungsten have focused on grain refinement, and grain boundary elongation through severe plastic deformation (SPD) techniques including high-pressure torsion (HPT) [35], equal channel angular extrusion (ECAE) [36] or pressing (ECAP) [37], rolling [4,21,22,38], swaging [39], and ball milling [40]. These works have illustrated the grain refining ability of severe plastic deformation (SPD) techniques applied to tungsten and the effects on mechanical behavior including increased hardness, increased strength, and reduction in the recrystallization and ductile-to-brittle-transition temperatures.

The limitations of common deformation processing methods provide an opportunity for relatively new SPD processing techniques that plastically strain (work) the material without a reduction in work-piece cross section area. Of these various methods, ECAE is the most promising due to the possibility of large sample dimensions, the uniformity of deformation, high strains capable with multiple processing steps, and the ability to control work-piece temperature, strain rate, and texture [22]. The authors use the acronym ECAE throughout this paper to be consistent with the nomenclature chosen by the originator of the method [41].

Previous work on processing tungsten for improved strength and ductility by ECAE has focused on high temperature deformation following a traditional approach. These studies were based on the idea of grain size refinement for strength and ductility improvements, and not the effects of texture and microstructure/grain elongation have involved deformation steps well above the nominal DBTT of tungsten. The results of this previous work have not been encouraging, in that no bulk tungsten has been produced with notable ductility or with a microstructure similar to that of wire or sheet. The objective of the current work was to identify a method for the fabrication of bulk tungsten with a tensile elongation to failure of at least 10%. By using ECAE processing at low temperature to produce an elongated microstructure, the current work demonstrates that fabrication of bulk polycrystalline tungsten with substantial tensile ductility is possible.

2. Materials and methods

Tungsten rods of commercial purity ~ 99.97% tungsten (W) manufactured by Plansee (Reutte, Austria) measuring 12 mm diameter by 50 mm in length were encapsulated in 25.4 mm square 304 stainless steel cans. The encapsulated as-received W rods were ECAE processed, using a 90° die angle, sliding wall tool, with a 0 ° outer die angle. Processing was done at 320 °C ± 10 °C at extrusion speeds less than 1.0 mm/s, with no rotation between extrusions (referred to as Route A).

Following ECAE, bend test specimens were sectioned from the processed bars (or billets) by wire electrical discharge machining (EDM) with the long axis of the test specimen along the ECAE extrusion direction into samples measuring ~ 2 × 1 × 14 mm^3. The EDM surface was removed by mechanical grinding followed by electrolytic polishing in a 1% NaOH solution.

Electron microscopy was conducted with an FEI Quanta 600 FE-SEM scanning electron microscope (SEM), with secondary and backscatter electron detectors. Characterization of the microstructure was done on the sample flow plane (side plane of extrusion billet). Quantizations of grain width and average subgrain diameter were accomplished using Fiji software formally known as ImageJ. Grain widths were measured at several locations on optical micrographs of etched samples. Average subgrain diameters were determined by averaging the length and width of as many as 500 individual grains for each specimen.

Because all samples were electro-polished prior to testing, it was possible to examine the deformed and fractured surfaces of specimens after testing without further surface preparation. Failure crack deflection angles were determined by measuring the angle between the loading direction and the average crack propagation direction.

Vickers hardness measurements were taken on the polished flow plane surface of small samples with a Leco Microhardness Tester LM300AT using a 300 g load and a loading time of 13 s. A total of 13 measurements were made on each sample. The highest and lowest values were disregarded when determining the average and standard deviation values.

Three-point bend tests were conducted with a custom-built test apparatus fabricated from H13 tool steel. The support pins were made from precision ground 0.20 mm diameter tungsten carbide (WC) pins. The distance between these roller supports was 7 mm as shown in Fig. 2. The sockets holding the WC rollers were coated with graphite to reduce friction. Rollers were held in grooved channels in the test

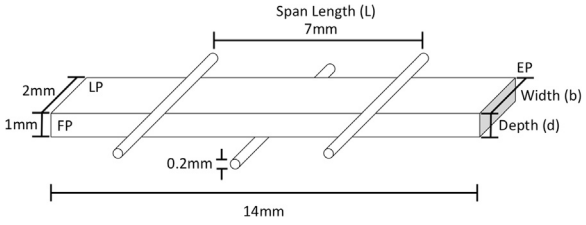

Fig. 2. Diagram of 3-point bend specimen and test apparatus configuration.

fixtures by thin nickel wire.

The bend tests were performed in an environmental chamber with temperature control. Temperature accuracy is based on the range of 95% confidence interval of chamber and surrogate specimen calibration. For temperatures above 300 °C, argon cover gas was used for oxidation protection. A refrigerant gas R152a, was used for controlling temperatures below ambient (20–25 °C). Samples were tested at a crosshead displacement speed of 0.01 mm s^{-1}, corresponding to a nominal strain rate of 0.001 s^{-1}, with the sample longitudinal plane (top plane of extrusion billet) normal to the loading direction as indicated in Fig. 2.

Determining stress and strain values from the bend tests was done with the load-displacement data and specimen dimensions using Eqs. (1) and (2).

$$\sigma_f = \frac{3FL}{2bd^2} \tag{1}$$

$$\varepsilon_f = \frac{6Dd}{L} \tag{2}$$

where σ_f is flexural stress, ϵ_f is flexural strain, F is applied load, L is span length, D is displacement, b is the sample width, and d is the sample depth. Flexural 0.002 offset strain yield and ultimate strengths were determined from the resulting stress-strain curves produced by Eq. (2) and 3. Flexural yield stress (FYS) was determined at 0.2% offset strain.

3. Results

3.1. Overview

To investigate the effects of ECAE processing on bulk polycrystalline tungsten both microstructure and mechanical behavior were characterized. Optical and scanning electron microscopy (SEM) were used to evaluate the microstructure. Average grain size, grain aspect ratio, subgrain size and subgrain aspect ratio were determined by individual measurements on no fewer than 500 individual grains and subgrains for each specimen. Mechanical characterizations were conducted through Vickers hardness measurements and 3-point bend testing.

Bend testing was conducted over a range of temperatures from ambient to ~ 500 °C. One measurement was done at −45 °C. Data from these tests consisted of load and displacement data converted into flexural stress and strain through 3-pont bend equations. Fracture energy was determined by integration of load-displacement curves normalized by the cross sectional area of the specimen.

3.2. Microstructure

Photomicrographs of the as-received (AR) and ECAE processed tungsten are shown in Fig. 3. The results of the characterized microstructures are summarized in Table 1. The optical micrographs seen in the left column of Fig. 3, show the elongation of the initial grain boundaries with each extrusion. The average grain width decreased from ~ 22 μm in the AR material, to ~ 5 μm by the fourth extrusion. Through the simple shear deformation of ECAE, each grain becomes more oriented along the extrusion direction, with an orientation of ~ 23° from the extrusion axis after the first extrusion to ~ 15° after the second, reaching ~ 7 ° after the forth extrusion.

Microstructural refinement is clearly visible in the series of electron micrographs shown in the middle column of Fig. 3 and the corresponding average subgrain diameter histograms shown in the right column. The AR material contains nearly equiaxed subgrains with an average diameter of 2.8 μm, and an aspect ratio near 2. During the ECAE process these subgrains are broken down. In the 1A material the microstructure exhibits banded regions, which are further divided/segmented into subgrains, with an average size of 0.9 μm and an aspect ratio of 3.6. The size distribution of these subgrains, shown in the 1A histogram indicates a peak at 0.4–0.6 μm. The microstructure of the 2A material is comprised of distinct regions with slightly differing subgrain sizes. The overall average subgrain width is 0.73 μm; the aspect ratio of these subgrains is 3.3. Comparing the upper left, middle and bottom right areas of the 2A electron micrograph, slight differences in microstructure can be seen. The plateau between 0.2 and 0.8 μm in the 2A subgrain sizes supports this observation of overlapping size distributions. Following four extrusions the microstructure is highly refined with an average subgrain size of ~ 0.65 μm, and a subgrain aspect ratio of 2.5. The subgrains of the 4A material are quite uniform in size with a narrow size distribution and a strong peak at 0.2–0.4 μm. The decrease in subgrain aspect ratio observed between the 1A, 2A and 4A materials is due to the increasing breakup and refinement of the tungsten grains rather than elongation through continued route A processing. The microstructure in the 4A material is similar to that of heavily drawn tungsten wire [42–44].

3.3. Mechanical properties

3.3.1. Overview

Three-point bend testing was used to investigate the effects of ECAE processing on mechanical behavior. This approach allowed characterization of the hardness, ductility, and strength. These tests were done using a custom-built test fixture located inside a temperature controlled three-zone clamshell furnace. Vickers hardness results are shown in Fig. 4. Selected flexural stress-strain curves for each processing condition for temperatures above and below the DBTT are shown Fig. 5. The results of these tests are summarized in Figs. 6–9; with total elongation (El) in Fig. 6, post-mortem bend specimen photographs in Fig. 7, flexural yield strength (FYS) in Fig. 8, and ultimate flexural strength (UFS) in Fig. 9. In all figures the results of repeated measurements are shown as average mean values with error bars indicating the standard deviation.

3.3.2. Hardness

Vickers hardness measurements were taken on the flow plane for each tungsten processing condition as shown in Fig. 4. In Fig. 4(a), the increase in Vickers hardness with successive extrusions is shown. The largest increase in hardness occurred during the first extrusion increasing from 425 HV in the AR condition to 535 HV. For two passes, the hardness increases to 570 HV. After flour passes, the hardness is 620 HV. This increase in hardness is likely due to a grain size strengthening affect, as evidenced by a Hall-Petch type relationship with subgrain size as shown in Fig. 4(b).

3.3.3. Ductility

The strain-strain curves for the AR material are shown in Fig. 5(a), and illustrate typical behavior for unworked polycrystalline tungsten at several temperatures below and above the DBTT. At room temperature the AR material possesses limited ductility, which does not begin to increase until the onset of the DBT near 150 °C, which can be seen in the summarized ductility data in Fig. 6. The ductility of the AR material increases rapidly with increasing temperature above ~ 150 °C, and by 250 °C is highly ductile. The ductile AR specimens are indicated by open symbols in Fig. 6, the onset and transition from ductile to brittle behavior of the AR material can be more qualitatively observed in the post-mortem specimen side-plane photos shown in Fig. 7.

The effect of initial ECAE processing (single pass (1A) material) can be seen in both the stress-strain diagrams in Fig. 5(b) as well as the summarized ductility data in Fig. 6. The initial ECAE extrusion results in very limited ambient temperature ductility. Samples routinely failed in a brittle manner prior to yielding even at temperatures near the DBT of the AR tungsten. The early brittle failure of the 1A specimens at these temperatures can be seen in the stress-strain curves below 205 °C in Fig. 5(b). With this decrease in ductility, the transition temperature is shifted to higher temperatures. In Fig. 5, the onset of the DBT for the 1A

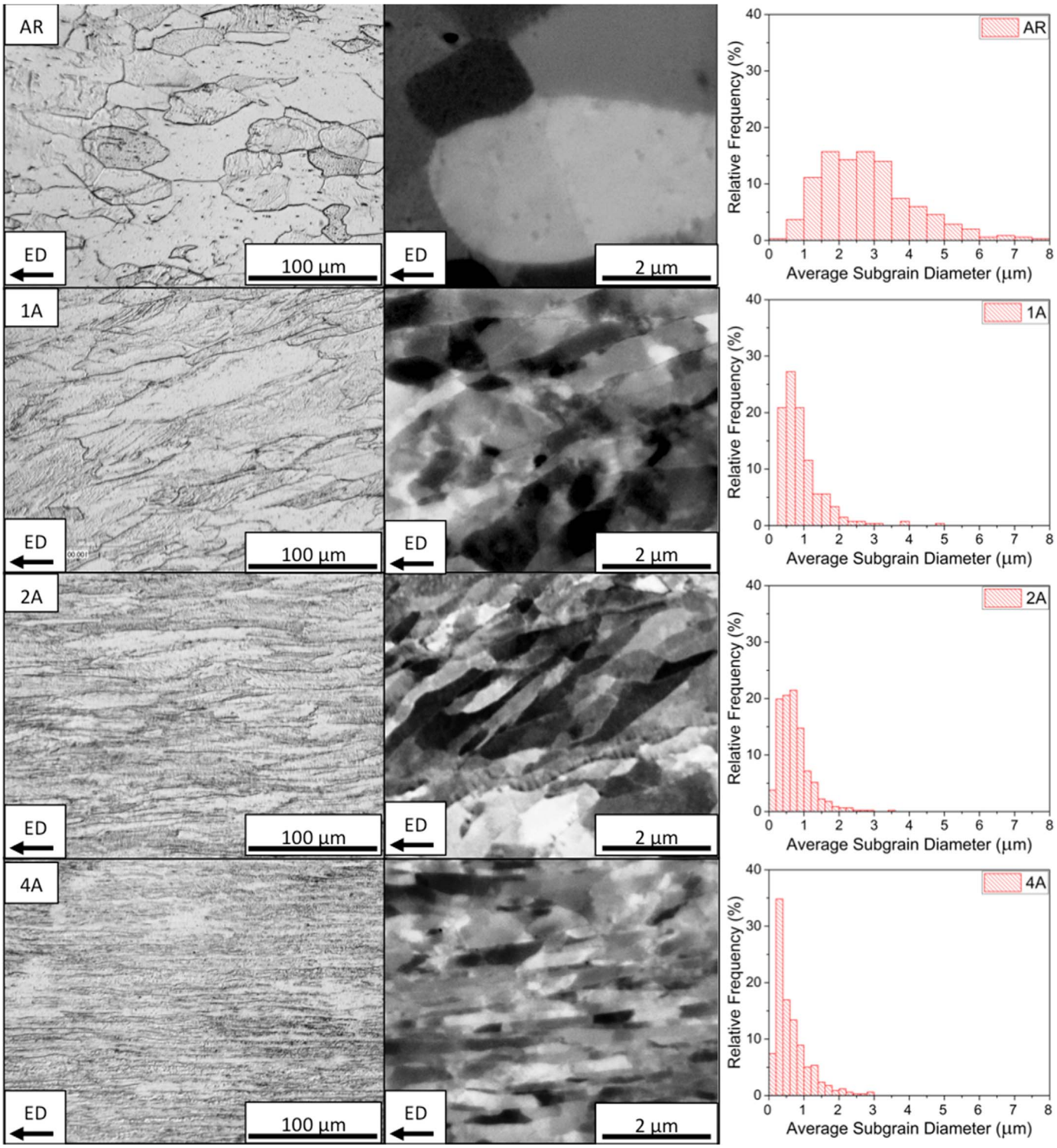

Fig. 3. (Left) Optical micrographs of as-received (AR) and ECAE processed tungsten. (Center) SEM images using a backscatter detector. (Right) Histograms of grain/subgrain size distribution. The images from top to bottom show the evolution of the microstructure from AR through four passes (strain of 4.6) of ECAE. ED denotes the extrusion direction.

material appears to occur above 200 °C. The decrease in ductility and shift in DBT can also be seen in the post-mortem 1A specimens, in Fig. 7. Below 225 °C, test specimens showed no permanent plastic deflection prior to failure and less than the AR material at greater temperatures.

The ductility of tungsten increases after a second extrusion. This two-pass (2A) material possessed greater room temperature ductility (near 2% El), and a decrease in the onset of the DBT from the AR material as shown by the stress-strain curves in Fig. 5(c), with some ductile behavior at 87 °C. In the summarized ductility data in Fig. 6, it is clear that the 2A material has higher baseline ductility than the AR material, with the onset of the DBT at near 100 °C. From the bend specimen images shown in Fig. 7, it can be seen that even at temperatures as low as 75 °C, some permanent deformation occurred during bend testing. The 2A material exhibits an increase in ductility with temperature indicating the presence of a DBT, however, the

Table 1
Summary of microstructure results and subgrain confidence interval (CI) for As-received and ECAE processed tungsten.

Processing	Strain (m/m)	Grain Width (μm)	Subgrain Diameter (μm)	95% Confidence Interval (CI) Subgrain Diameter (μm)	Subgrain Aspect Ratio
AR	0	22 ± 10	2.83 ± 1.33	2.69–2.97	2.0 ± 0.9
1A	1.15	15 ± 9	0.90 ± 0.62	0.83–0.98	3.6 ± 2.1
2A	2.3	8 ± 4	0.73 ± 0.45	0.69–0.78	3.3 ± 1.9
4A	4.6	5 ± 3	0.65 ± 0.50	0.60–0.70	2.5 ± 1.4
Wire	–	5 ± 3	1.9 ± 1.4	–	4 ± 2

increase is smaller than that of the AR material, and is similar to the behavior of the 1A material. The ductility of the 2A material also reaches a ductility plateau at around 20% at temperatures above 300 °C. This is similar to the other worked materials at similar temperatures.

Tungsten processed by 4A ECAE passes has the best mechanical properties of all cases examined. At room temperature the average total elongation of the 4A material was between 17% and 23% El, with an average of 19% EL. The extent of this elongation is seen in the stress-strain graphs in Fig. 5(d), while the total elongation of each specimen at testing temperature can be seen in Fig. 6, as well as the post-mortem specimens in Fig. 7. Because of this extreme level of ductility at ambient temperature, further testing was done at −45 °C in order to better identify the onset of ductility. At this temperature the 4A material possessed a ductility of 13% El. From this it was concluded that the onset of ductile behavior in 4A tungsten is bellow −45 °C. The dashed line above the −45 °C specimen in Fig. 7 indicates this point. Above room temperature it was noted that the ductility varies only slightly from 24 °C to 100 °C remaining near 20% El, and then increases to approximately 30% between 100 and 200 °C. Further increasing the test temperature caused the ductility to decrease to 20% El at 250 °C, and 15% El above 400 °C. This rise and fall in ductility indicates the presence of differing deformation or failure mechanisms above and below the peak in ductility. The effect of this increase and decrease in ductility is clearly seen in the bend angle of the post-test specimens shown in Fig. 7, and in the total elongation at 175 °C and 205 °C in the stress-strain curves in Fig. 5(d).

The changes in deformation behavior with temperature can be seen in the optical images of post-tested samples shown in Fig. 7. Images were taken on the extrusion flow plane. The specimen fracture crack path is highlighted by a white line for samples that failed without significant deformation. Specimens absent from this collection of images were unrecovered (lost) following testing, due to their energetic failure. In permanently deformed samples, the brighter areas indicate the region that experienced significant plastic deformation during testing. The image contrast change in the plastically deformed region is caused by the contraction/expansion of material in either tension or compression, altering the surface morphology resulting in an increase or decrease in reflected light into the detector. It should be noted that in the AR material this region is much larger than that of the worked materials, even at similar bend angles. In general, the deformed area for all specimens increases with temperature. The exception to this occurs in the 4A material, where the deformed area above 250 °C decreases, a possible indication of an alternate deformation mechanism due to the high degree of working.

3.3.4. Yield strength

The flexural yield stress (FYS) values or each processing condition at all temperatures tested are shown in Fig. 8. Values with error bars indicate the mean and standard deviation of multiple data point measurements. The 4A material possesses the highest FYS over the entire temperature range, with a room temperature value greater than 3000 MPa. The 2A material possesses the next highest room temperature YS ~ 2250 MPa, followed by the AR material at 2000 MPa. The 1A case had the lowest YS of less than 1000 MPa. The 1A material differs from the others as the FYS increased from 24 °C to 150 °C, approaching the strength of 2A material at 150 °C. Beyond 150 °C the material behaves similarly to the 2A material. The highest observed FYS of 3300 MPa is observed in the 4A specimen at −45 °C. The YS of the 4A and 2A materials decreased approximately 2000 MPa between room temperature and 400 °C. Below 150 °C the FYS of the AR material is approximately 1700 MPa, but then decreases to 1200 MPa over a 100 °C temperature range. Above 250 °C the rate at which FYS decreased is less than 250 MPa above 400 °C. There also appears to be a noticeable drop in the FYS of the 4A material near 200 °C. However, due to the relatively small size of this decrease and the lack of repeated tests in this region, it is not possible to draw a statistically significant conclusion and this apparent relatively sharp decline should be verified by additional tests.

3.3.5. Ultimate flexural strength

The ultimate flexural strength (UFS) results plotted against temperature for all tungsten processing conditions are shown in Fig. 9, with error bars indicating standard deviations from multiple tests. Similar to the FYS results, the 4A-processed tungsten had the highest UFS, with an ambient temperature strength of 3900 MPa. The high UFS strength at room temperature is followed by the 2A material (2550 MPa), the AR

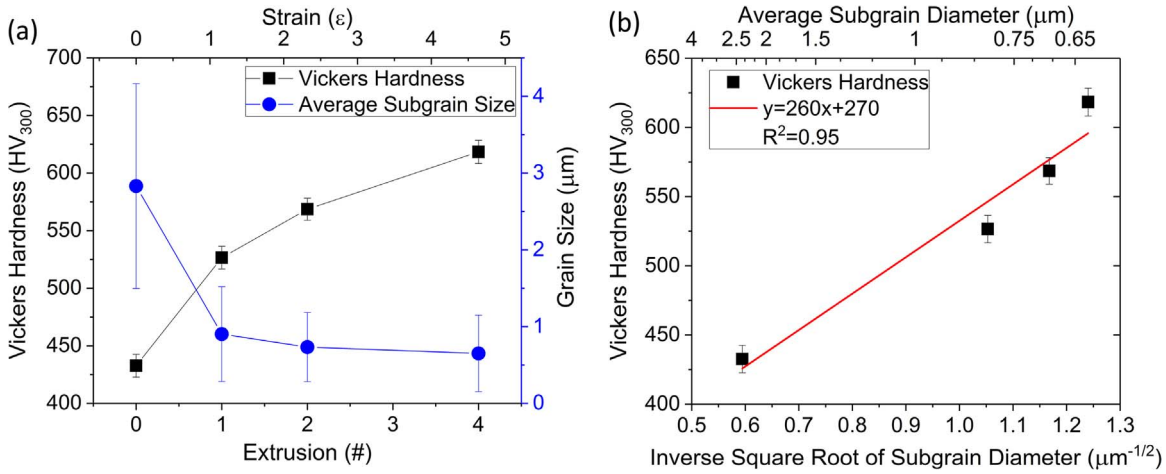

Fig. 4. (a) Ambient temperature Vickers hardness and average subgrain size values plotted by extrusion number and plastic strain (top axis). (b) Hall-Petch plot of Vickers hardness data. The Vickers hardness measurements were taken on the flow plane.

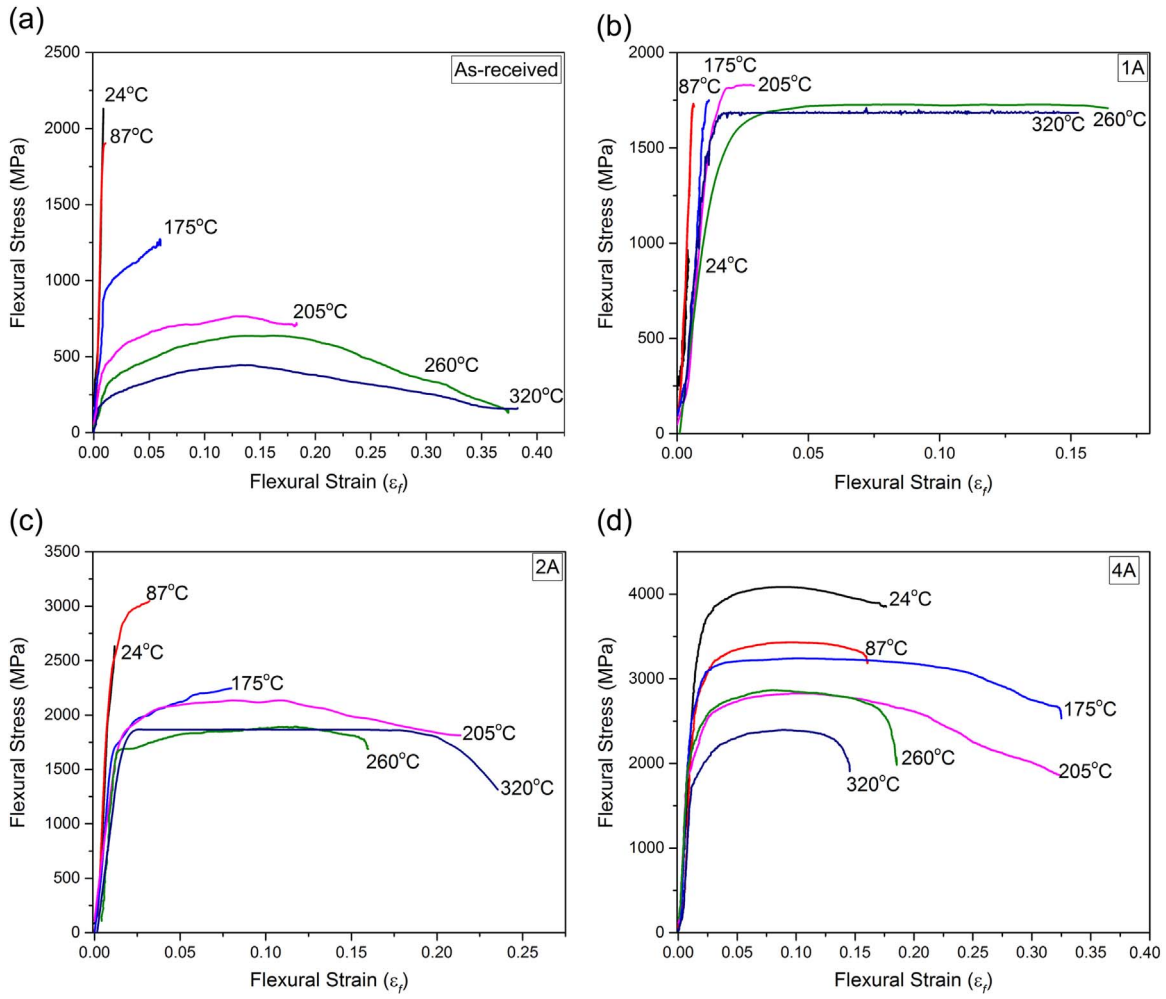

Fig. 5. Stress-strain curves for as-received and ECAE processed tungsten derived from 3-point bend testing: (a) as received, (b) 1A, (c) 2A, and (d) 4A. The testing strain rate is estimated to be 0.001 s^{-1}. Note horizontal scales are not the same for figures a-d. This scale variation enables a better comparison between data sets.

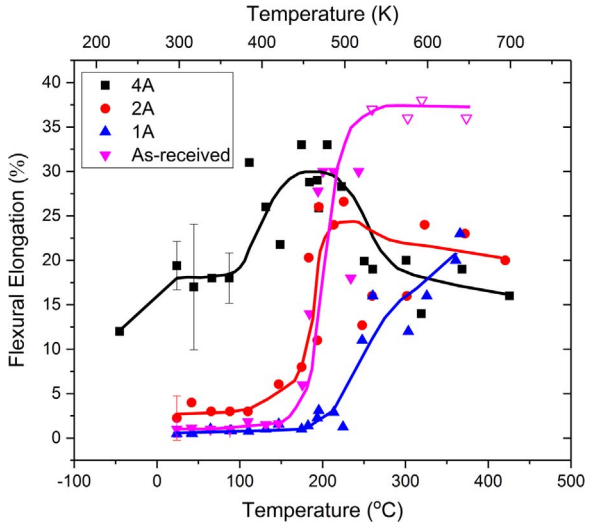

Fig. 6. Elongation to failure results of tungsten specimens under 3-point bend testing. Open symbols indicate samples that did not fail during testing (displacement was limited by the test fixture).

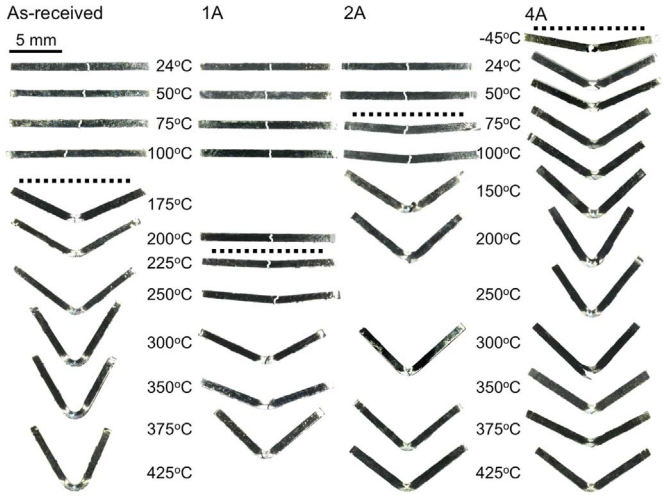

Fig. 7. Side view (flow plane) optical micrographs of 3-point bend test specimens after testing. The dashed lines indicate the onset of ductility. The specimen length is 14 mm.

material (2000 MPa), and finally the 1A tungsten (940 MPA). The UFS temperature behavior is very similar to that observed for FYS, with some slight differences. In the 4A material an increase in UFS between −45 °C and 24 °C was observed as well as a less significant decrease in UFS before the DBTT 200–300 °C. The 4A material also retained a significantly higher UFS than the other worked materials, a nearly 1000 MPa difference above 250 °C. Also, the standard deviation between multiple measurements is smaller than those for the FYS

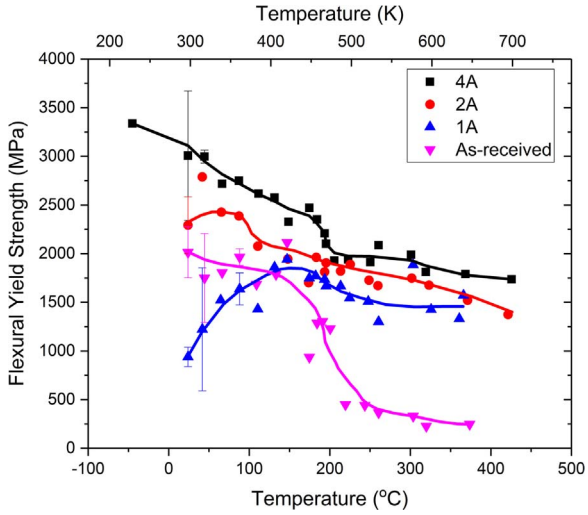

Fig. 8. Flexural yield stress (FYS) results of tungsten determined by 3-point bend testing. This yield stress is for 0.2% offset strain. Error bars indicate the nominal standard deviation of multiple sample measurements at a given temperature.

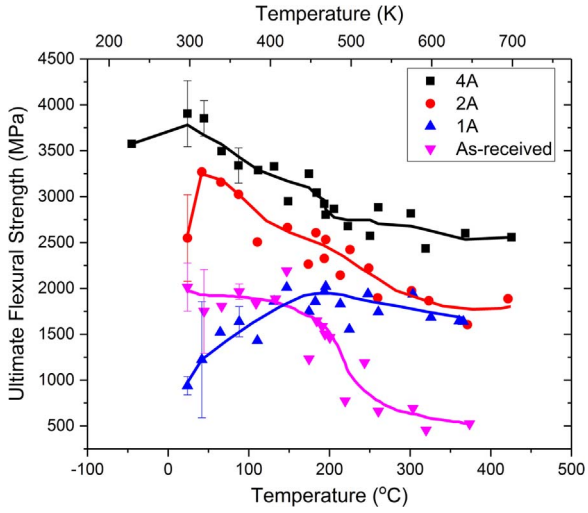

Fig. 9. Ultimate flexural strength (UFS) results for as-received, 1A, 2A and 4A ECAE processed tungsten bend specimens. The UFS values are derived from the maximum stress values from corresponding stress-strain curves.

measurements.

3.4. Texture

Crystallographic texture maps in the as-received and 4A processed tungsten are shown in electron back scatter diffraction (EBSD) micrographs in Fig. 10. The as-received material appears weakly textured while the 4A material has strong {110} and {111} texture orientations along the extrusion direction.

4. Discussion

4.1. Processing

Through ECAE processing, bulk polycrystalline tungsten was severely plastically deformed to greater amounts of strain at lower temperatures than previously reported. The processing done in this work is identified in Fig. 1, as the set of circled data points in the lower left quadrant of the figure. Most notable, the tungsten processing reported here was conducted at near 300 °C, which is below all other methods at similar amounts of total accumulated stain. The only tungsten processed by others at similar temperatures had a prior accumulated strain greater than 8.

The success of our processing approach is likely due to the influence of strain rate, deformation mechanics, and stress state during processing. The strain rate behavior of tungsten has been examined previously [45–49], especially the alteration of the DBTT with strain rate [9–11,45]. Based on this, it can be assumed that the very slow strain rate used for processing here reduced the DBTT sufficiently to permit plastic deformation without fracture, possibly through a creep like deformation behavior, where dislocations had sufficient time to slip, climb, and reorganize during processing. The simple shear processing caused by ECAE may have also enabled this successful processing because this method minimizes tensile strain in the work piece during extrusion. The hydrostatic stress imposed on the tungsten by steel material encapsulation during extrusion is another possible explanation of the successful processing. Encapsulation combined with tight extrusion chamber dimensions impose a compressive stress to the work piece during processing and decreases the opportunity for tensile stress and the formation and propagation of cracks during processing.

Besides producing high ductility at room temperature, the 4A ECAE processed tungsten also shows a substantial increase in strength when compared to the as-received material as shown in Figs. 8 and 9. The improved mechanical behavior is attributed to the microstructure and texture features produced by the severe plastic deformation processing: a higher dislocation density, refined subgrains, elongation/orientation of grain boundaries, and orientation of the {101} and {111} planes seen in Fig. 10.

4.2. Microstructure

As seen in this work, ECAE processing is an effective tool for altering the microstructure of polycrystalline tungsten. At the smallest size scale, ECAE generates numerous dislocations increasing their density several orders of magnitude from the as-received (AR) annealed state. This is due to the large strain imparted with a single extrusion ~ 1.15, but also, the relatively low homologues temperature $\sim 0.16\ T_m$ of processing, which inhibits defect motion and annihilation during processing. The presence of these dislocations may explain the shift in ductility, and FE values to greater temperatures in the 1A material. Similar observations have been made and attributed to preexisting dislocations in both single [8] and polycrystalline tungsten [19]. It may be that this is not observed in the 2A and 4A materials which have similar concentrations of dislocations because they possess sufficient grain boundary orientation, elongation, texturing, and subgrain refinement to compensate for the pinning effects of a higher dislocation density.

Subgrain refinement through ECAE processing appears to significantly increase the strength and hardness of tungsten, as seen in both stress-strain curves and Vickers hardness results. The Hall-Petch type behavior of the subgrain size and Vickers hardness trend supports this assertion. Refinement of the initial AR subgrains may also contribute to the change in failure mode observed between the AR and worked materials. The larger subgrains in the AR material provide a low energy path for crack propagation, while in the highly refined material with smaller subgrains, the as-worked material provides forces a tortuous path for crack propagation and thus transgranular cleavage competes with intergranular separation as the dominate fracture mode.

The distinction between grains and subgrains is normally defined by the angle of misorientation between adjacent grains. Single crystal regions with grain orientations less than 15° between adjacent grains are considered subgrains. However, without the availability of TEM or EBSD images sufficient to resolve dislocation structures, it is difficult to determine the exact nature of the grains and subgrains for our ECAE processed materials. Never the less, optical and scanning electron micrographs do provide some insight. The well-defined grain boundaries and faceted grains in the AR material optical micrographs indicate that

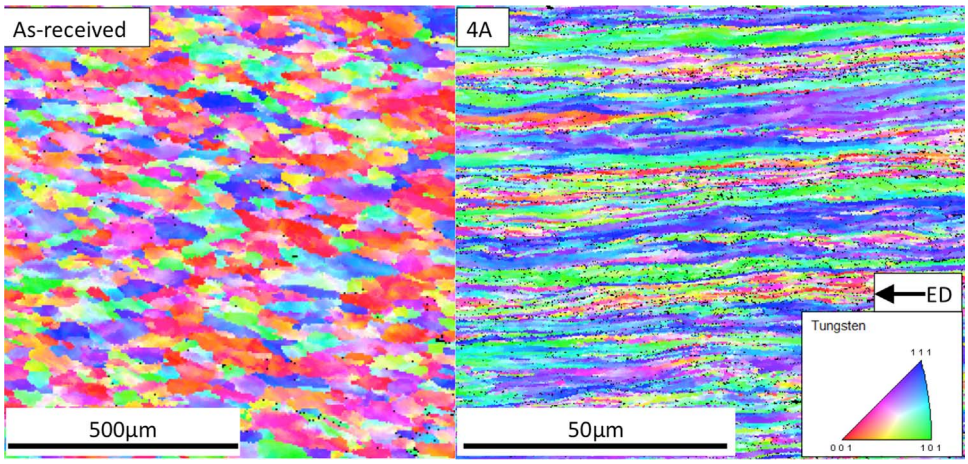

Fig. 10. EBSD maps of texture orientation for as-received and 4A processed tungsten.

these are recrystallized grains. The presence of etched grain boundaries also suggests these are in fact grains with high angle grain boundaries, as the boundaries are preferentially attacked during electrolytic etching. The absence of substantial boundary etching within these "grain" regions but the presence of etching along the initial deformed grain boundaries indicates that the within grain features seen in the SEM micrographs are subgrains with low angle boundaries. The same holds true for the worked material – with the caveat that working may have produced regions of sufficient grain boundary misorientation to technically classify some of the refined subgrains as grains. The lamella like structure observed in the 4A material suggests anisotropic behavior.

4.3. Mechanical behavior

4.3.1. Hardness/strength

The hardness and strength of both AR and ECAE processed polycrystalline tungsten are primarily dictated by the subgrain size. The Vickers hardness results clearly indicate a dependence on subgrain size through a Hall-Petch type relationship – see Fig. 4. Strengthening due to grain size refinement is also responsible for the greater FYS and UFS of the ECAE processed material, as strength follows a trend similar to the hardness observations.

The decreases in both FYS and UFS with temperature for AR and ECAE processed tungsten are expected, because more energy is available at elevated temperature to assist dislocation motion. The higher retained strength of the ECAE processed tungsten must be due to their finer microstructure and higher dislocation density. In the AR material a dramatic decrease in strength occurs at temperatures near the DBTT, an indication of additional slip system activation requiring less energy and thus a lower flow stress. The presence of a similar drop in the 4A material but absence in the other ECAE processed tungsten materials suggests that other factors such as texture and loading direction may influence the ability for dislocation motion to accommodate strain.

4.3.2. Grains size, ductility and the DBTT

There has been substantial research into the grain size effect on mechanical properties of tungsten, and the findings of this study confirm that grain size has a significant impact on hardness and yield strength. However, the grain size impact on ductility does not appear to contribute as significantly as either texture and grain morphology, contrary to the assertions made by Reiser et al. [4]. It appears that the relationship between grain size and ductility is one of correlation and not causation. The grain refinement typically observed in tungsten wire processing that improves ductility also produces the morphological and texture features that impart ductility, e.g. ECAE, rolling, and drawing. If ductility did have a strong dependence on grain size the 2A and 4A materials would have similar ductility, because the difference in subgrain sizes for these two cases is small (~ 0.08 µm). However, this is not the case, and the ductility differs by an order of magnitude between the two materials at room temperature.

The intent of this project was not to determine whether or not SPD processing influences the ductile-to-brittle transition temperature (DBTT) of pure tungsten. Our suspicion is that if we had done appropriate testing, we would have seen at most a modest reduction in the DBTT with the level of work (plastic strain). This assertion is based on the flexural elongation results presented in Fig. 6: the flexural elongation at failure as a function of temperature for AR material follows a trend characteristic of material with a clear DBTT – ductile at temperatures above about 250 °C with a transition to fully brittle behavior by ~ 175 °C. It is fortuitous that this transition temperature range is similar to the published DBTT (200–300 °C) for tungsten. The transition temperature ranges for the 1A and 2A materials are ~ 225–400 °C and 125–200 °C respectively – an apparent increase in DBTT for the1A material and decease for the 2A material. The AR and 1A materials show virtually no ductility below ~ 150 °C and ~ 200 °C respectively. The 2A material on the other hand exhibits modest ductility (2–3%) below ~ 125 °C. The flexural elongation to failure curve for the 4A material is curious: substantial ductility (> 10%) at −45 °C with an apparent plateau peak at ~ 125–225 °C with a drop above ~ 225 °C. These results indicate a substantial drop in the DBTT for the 4A material if the DBTT is determined by this method. However, because determination of the DBTT temperature involves high strain rate testing (Charpy impact), which was not done here, this interpretation is most likely false. To further complicate a determination of the DBTT from the elongation to failure results, the data show significant scatter in the transition temperature range. Never the less, because of the large number of individual tests performed, we have confidence in the flexural elongation with temperature trends described. Further work on determination of the DBTT of the worked tungsten samples is underway.

5. Summary/conclusion

5.1. Summary

Commercially pure polycrystalline tungsten was successfully processed to strains exceeding 4.5 at a low homologous temperature by multipass ECAE. This processing resulted in bulk material with submicron subgrains and a highly elongated microstructure. The hardness of this tungsten exhibits a Hall-Petch type relationship with the average subgrain diameter. Material processed to a strain of ~ 4.6 has a room temperature strength exceeding 3 GPa, and exceptionally high room temperature ductility with observed total elongations between 17% and

23% at failure. This processing also produced a strong {110} and {111} texture along the extrusion direction for the most heavily worked material. The approach developed in this work to refine microstructure and increase ductility and toughness in bulk tungsten may be a useful strategy for improving the mechanical properties of other brittle crystalline metals.

5.2. Conclusions

Based on the results of this work, the following conclusions can be drawn:

1. The results show that it is possible to develop a lamellar microstructure in bulk tungsten similar to that of drawn tungsten wire.
2. It is possible to develop a texture in bulk tungsten with strong {110} and {100} components similar to that of drawn tungsten wire.
3. Decreasing the tungsten subgrain size increases strength and hardness without significantly deceasing ductility and the DBTT.
4. There are two factors that enable ductility in polycrystalline bulk tungsten: a microstructure that resists premature failure by inhibiting fracture, and a favorable texture with active slip systems that permit dislocation mobility.
5. From stress-strain data and optical micrographs, it appears that work hardening in ECAE processed tungsten is limited and the primary mode of deformation is flow localization.
6. The presence of {111} and {110} texture in tungsten enables sufficient dislocation mobility to permit substantial deformation.
7. Polycrystalline tungsten with a lamellar microstructure exhibits ductility characteristics similar to {110} oriented single crystal material.
8. Severely plastically deformed bulk tungsten can possesses significant ductility far below the apparent DBTT.
9. The lamellar microstructure in the 4A material suggests this ductile material will have anisotropic mechanical behavior.

Acknowledgements

The authors thank Robert Barber for his aid in ECAE processing and David Foley and Ankit Srivastava for their fruitful discussions. Financial support from the SMART scholarship program and the Army through contract W15QKN15C0031 to Shear Form, Inc. is gratefully acknowledged.

References

[1] E. Lassner, W.-D. Schubert, Tungsten: Properties, Chemistry, Technology of the Elements, Alloys, and Chemical Compounds, Springer Science & Business Media, New York, 1999.
[2] Z. Li, R.G. Gordon, D.B. Farmer, Y. Lin, J. Vlassak, Nucleation and adhesion of ALD copper on cobalt adhesion layers and tungsten nitride diffusion barriers, Electrochem. Solid-State Lett. 8 (2005) G182–G185.
[3] Q. Yan, X. Zhang, T. Wang, C. Yang, C. Ge, Effect of hot working process on the mechanical properties of tungsten materials, J. Nucl. Mater. 442 (2013) S233–S236.
[4] J. Reiser, J. Hoffmann, U. Jäntsch, M. Klimenkov, S. Bonk, C. Bonnekoh, et al., Ductilisation of tungsten (W): on the shift of the brittle-to-ductile transition (BDT) to lower temperatures through cold rolling, Int. J. Refract. Met. Hard Mater. 54 (2016) 351–369.
[5] Y. Zhang, A.V. Ganeev, J.T. Wang, J.Q. Liu, I.V. Alexandrov, Observations on the ductile-to-brittle transition in ultrafine-grained tungsten of commercial purity, Mater. Sci. Eng.: A 503 (2009) 37–40.
[6] H. Yuan, Y. Zhang, A.V. Ganeev, J.T. Wang, I.V. Alexandrov, Strengthening and toughening effect on tungsten subjected to multiple ECAP, Nanomaterials by Severe Plastic Deformation: Nanospd5, Pts 1 and 2, 667–669 Trans Tech Publications Ltd, Stafa-Zurich, 2011, pp. 701–706.
[7] D. Rupp, S. Weygand, Anisotropic fracture behaviour and brittle-to-ductile transition of polycrystalline tungsten, Philos. Mag. 90 (2010) 4055–4069.
[8] P. Gumbsch, Brittle fracture and the brittle-to-ductile transition of tungsten, J. Nucl. Mater. 323 (2003) 304–312 (Dec).
[9] G. Subhash, Y.J. Lee, G. Ravichandran, Plastic deformation of CVD textured tungsten—I. constitutive response, Acta Metall. Mater. 42 (1994) 319–330 (1994/01/01).
[10] G. Subhash, Y. Lee, G. Ravichandran, Plastic deformation of CVD textured tungsten—II. Characterization, Acta Metall. Et. Mater. 42 (1994) 331–340.
[11] A. Giannattasio, S.G. Roberts, Strain-rate dependence of the brittle-to-ductile transition temperature in tungsten, Philos. Mag. 87 (2007) 2589–2598.
[12] P.P. Bourque, D.F. Bahr, M.G. Norton, Effect of thermal treatment on failure modes in tungsten wire, Mater. Sci. Eng.: A 298 (2001) 73–78.
[13] G. Hahn, A. Gilbert, R. Jaffee, The effects of solutes on the ductile-to-brittle transition in refractory metals, Battelle Memorial Inst. Defense Metals Information Center, Columbus, Ohio, 1962.
[14] J.H. Schwertz, C.P. Muller, W.A. McNeieh, Tungsten sheet rolling program, DTIC Document, 1967.
[15] B. Gludovatz, S. Wurster, A. Hoffmann, R. Pippan, Fracture toughness of polycrystalline tungsten alloys, Int. J. Refract. Met. Hard Mater. 28 (2010) 674–678 (Nov).
[16] A. Giannattasio, Z. Yao, E. Tarleton, S.G. Roberts, Brittle-ductile transitions in polycrystalline tungsten, Philos. Mag. 90 (2010) 3947–3959 (2010).
[17] M. Rieth, A. Hoffmann, Influence of microstructure and notch fabrication on impact bending properties of tungsten materials, Int. J. Refract. Met. Hard Mater. 28 (2010) 679–686.
[18] P. Gumbsch, J. Riedle, A. Hartmaier, H.F. Fischmeister, Controlling factors for the brittle-to-ductile transition in tungsten single crystals, Science 282 (1998) 1293–1295.
[19] D. Rupp, R. Mönig, P. Gruber, S. Weygand, Fracture toughness and microstructural characterization of polycrystalline rolled tungsten, Int. J. Refract. Met. Hard Mater. 28 (2010) 669–673.
[20] J. Reiser, S. Wurster, J. Hoffmann, S. Bonk, C. Bonnekoh, D. Kiener, et al., Ductilisation of tungsten (W) through cold-rolling: r-curve behaviour, Int. J. Refract. Met. Hard Mater. 58 (2016) 22–33.
[21] Q. Wei, L.J. Kecskes, Effect of low-temperature rolling on the tensile behavior of commercially pure tungsten, Mater. Sci. Eng.: A 491 (2008) 62–69.
[22] X. Zhang, Q. Yan, S. Lang, M. Xia, C. Ge, Texture evolution and basic thermal--mechanical properties of pure tungsten under various rolling reductions, J. Nucl. Mater. 468 (2016) 339–347.
[23] M. Faleschini, H. Kreuzer, D. Kiener, R. Pippan, Fracture toughness investigations of tungsten alloys and SPD tungsten alloys, J. Nucl. Mater. 367–370 (2007) 800–805.
[24] W.D. Coolidge, Tungsten and method of making the same for use as filaments of incandescent electric lamps and for other purposes, ed: Google Patents, 1913.
[25] Z. Jeffries, Metallography of tungsten, Trans. Am. Inst. Min. Metall. Eng. 60 (1919) 588–643.
[26] D. Lee, Fracture of drawn tungsten wires, Metall. Trans. A 6 (1975) 2083–2088.
[27] B. Ma, Q.-H. Rao, Y.-H. He, Effect of crystal orientation on tensile mechanical properties of single-crystal tungsten nanowire, Trans. Nonferrous Met. Soc. China 24 (2014) 2904–2910.
[28] K.-c.i. Li, Tungsten, its History, Geology, Ore-Dressing, Metallurgy, Chemistry, Analysis, Applications, and Economics, Reinhold Publishing Corporation, New York, 1955.
[29] C.J. Smithells, Tungsten its Metallurgy, Properties, and Applications, New York, Chemical Pub. Co., New York, 1953.
[30] S.W.H. Yih, C.T. Wang, Tungsten: Sources, Metallurgy, Properties, and Applications, Plenum Press, New York, 1979.
[31] V. Thompson, V. Petersen, Research on workable refractory alloys of tungsten, tantalum, molybdenum, and columbium, DTIC Document, 1963.
[32] L.J. Kecskes, K.C. Cho, R.J. Dowding, B.E. Schuster, R.Z. Valiev, Q. Wei, Grain size engineering of bcc refractory metals: top-down and bottom-up—application to tungsten, Mater. Sci. Eng.: A 467 (2007) 33–43.
[33] G.C.J. Bodine, Tungsten sheet rolling program. Final Report, June 1, 1960-March 1, 1963, N63-14854 United StatesTue Feb 05 15:08:31 EST 2008DTIE, NSA-18-025944English, 1963.
[34] A.V. Ganeev, R.K. Islamgaliev, R.Z. Valiev, Refinement of tungsten microstructure upon severe plastic deformation, Phys. Met. Metallogr. 115 (2014) 139–145.
[35] Y. Zhang, A.V. Ganeev, X. Gao, A.V. Sharafutdinov, J.T. Wang, I.V. Alexandrov, Influence of HPT deformation temperature on microstructures and thermal stability of ultrafine-grained tungsten, in: Y. Estrin, H.J. Maier (Eds.), Nanomaterials by Severe Plastic Deformation Iv, Pts 1 and 2, 584–586 Stafa-Zurich: Trans Tech Publications Ltd, 2008, pp. 1000–1005.
[36] Y. Zhang, A.V. Ganeev, J.T. Wang, J.Q. Liu, I.V. Alexandrov, Observations on the ductile-to-brittle transition in ultrafine-grained tungsten of commercial purity, Mater. Sci. Eng.: A 503 (2009) 37–40.
[37] R.Z. Valiev, T.G. Langdon, Principles of equal-channel angular pressing as a processing tool for grain refinement, Prog. Mater. Sci. 51 (2006) 881–981 (9//).
[38] Q. Wei, L.J. Kecskes, K.T. Ramesh, Effect of low-temperature rolling on the propensity to adiabatic shear banding of commercial purity tungsten, Mater. Sci. Eng.: A 578 (2013) 394–401.
[39] R.W. Margevicius, J. Riedle, P. Gumbsch, Fracture toughness of polycrystalline tungsten under mode I and mixed mode I/II loading, Mater. Sci. Eng.: A 270 (1999) 197–209 (9/30).
[40] R. Malewar, K. Kumar, B. Murty, B. Sarma, S. Pabi, On sinterability of nanostructured W produced by high-energy ball milling, J. Mater. Res. 22 (2007) 1200–1206.
[41] V.M. Segal, Materials processing by simple shear, Mater. Sci. Eng.: A 197 (1995) 157–164.
[42] A. Funkenbusch, F. Bacon, D. Lee, The influence of microstructure on fracture of drawn tungsten wire, Metall. Trans. A 10 (1979) 1085–1091.
[43] D.B. Snow, The recrystallization of commercially pure and doped tungsten wire drawn to high strain, Metall. Trans. A 10 (1979) 815–821.
[44] P. Schade, Wire drawing failures and tungsten fracture phenomena, Int. J. Refract. Met. Hard Mater. 24 (2006) 332–337.

[45] A. Chilton, A. Wronski, The effects of strain rate and pressurization on the ductile-brittle transition temperature of polycrystalline sintered tungsten, J. Less Common Met. 17 (1969) 447–450.
[46] Q. Wei, L.J. Kecskes, Effect of low-temperature rolling on the tensile behavior of commercially pure tungsten, Mater. Sci. Eng. a-Struct. Mater. Prop. Microstruct. Process. 491 (2008) 62–69 Sep 15.
[47] Z. Pan, Y.Z. Guo, S.N. Mathaudhu, L.J. Kecskes, K.T. Hartwig, Q. Wei, Quasi-static and dynamic mechanical properties of commercial-purity tungsten processed by ECAE at low temperatures, J. Mater. Sci. 43 (2008) 7379–7384 Dec.
[48] W.S. Lee, C.F. Lin, G.L. Xiea, Dynamic shear deformation and failure behaviour of pure polycrystalline tungsten, Mater. Sci. Eng. a-Struct. Mater. Prop. Microstruct. Process. 247 (1998) 102–112 (Jun 1).
[49] T. Dümmer, J. Lasalvia, G. Ravichandran, M. Meyers, Effect of strain rate on plastic flow and failure in polycrystalline tungsten, Acta Mater. 46 (1998) 6267–6290.